JOURNAL OF AIRCRAFT
Vol. 31, No. 5, Sept.–Oct. 1994

Numerical Simulation of Steady and Unsteady, Vorticity-Dominated Aerodynamic Interference

Jamal M. Elzebda,* Dean T. Mook,† and Ali H. Nayfeh‡
Virginia Polytechnic Institute and State University, Blacksburg, Virginia 24061

The problem of modeling steady and unsteady aerodynamic interference is discussed. A configuration resembling the X-29 is used as an example. The general unsteady vortex-lattice method is used to model the flowfield. By considering the components operating alone and as members of the complete configuration, we demonstrate the importance of accurately simulating the wakes of the upstream components. The wakes of the canards as well as the canards themselves have a strong negative influence on the lift generated by the main wing; the main wing has a positive influence on the lift generated by the canards. The forward sweep of the main wing tends to focus the generated upwash in the vicinity of the canards. It is shown that the maximum influence of the vorticity shed from the canards does not develop until the shed vorticity convects downstream directly over the main wing. The general unsteady vortex-lattice method appears to be a reasonably accurate model of closely coupled, vorticity-dominated flowfields as long as the lines of the separation are known and vortex bursting does not occur near the wings.

I. Introduction

THE long-standing problem of modeling aerodynamic interference has become more difficult.[1] Modern configurations of high-performance aircraft often employ canards, and the vorticity continuously being shed from their tips, trailing edges, and possibly leading edges typically passes close to the main wing. In order to accurately model aerodynamic interference in these vorticity-dominated flowfields, one must be able to determine the strength, orientation, and location of the vorticity in the wakes of the upstream components. In this article we describe the use of the general unsteady vortex-lattice method to model both steady and unsteady interference. And we select as an example the flowfield around a configuration resembling the X-29. The general unsteady vortex-lattice method is not restricted by planform, angle of attack, or curvature of the lifting surfaces as long as the lines of separation are known and vortex bursting does not occur in the near vicinity of the configuration.

The vortex-lattice method captures many of the features of the flowfield. There is good agreement between numerical and experimental values of the lift and drag on the complete configuration in steady flow. We consider each component when it is operating alone and when it is operating as part of the complete configuration. We find that the wakes of the canards as well as the canards themselves have a negative influence on the lift generated by the main wing and that, in contrast, the main wing has a positive influence on the lift generated by the canards. The forward sweep of the main wing tends to focus the upwash it generates in the vicinity of the canards, and thereby enhance its positive influence on them. For a rearward sweep, the positive influence of the main wing on the canards would be diffused.

Two unsteady flows are considered: 1) a smooth ramp up in the angle of attack of the canards while the angle of attack of the main wing remains constant, and 2) a simple-harmonic variation in the angle of attack of the canards while the main wing remains fixed. The present simulations predict differences in the times when the maxima of the loads occur and the times when the maxima of the deflections of the canards occur; the phases are clearly evident in the present results. The time-varying influence of the vorticity shed from the canards on the main wing is demonstrated.

II. Aerodynamic Model

The basis for the method is the definition of vorticity, $\boldsymbol{\Omega}$, and the definition of incompressible flow

$$\boldsymbol{\Omega} = \operatorname{curl} \boldsymbol{v} \tag{1}$$

$$\operatorname{div} \boldsymbol{v} = 0 \tag{2}$$

where $\boldsymbol{v}$ is the velocity field. Equations (1) and (2) can be solved to give $\boldsymbol{v}$ as a function of $\boldsymbol{\Omega}$

$$\boldsymbol{v}(\boldsymbol{r}_p, t) = \frac{1}{4\pi} \int\int\int \frac{\boldsymbol{\Omega}(\boldsymbol{r}_s, t) \times (\boldsymbol{r}_p - \boldsymbol{r}_s)\, d\tau(\boldsymbol{r}_s)}{|\boldsymbol{r}_p - \boldsymbol{r}_s|^2} \tag{3}$$

where $\boldsymbol{r}_p$ is the point at which the velocity is being calculated, t is the time, the integration is carried out over the volume of the flowfield as well as the interior of any rotating bodies, $\boldsymbol{r}_s$ is the location of the vorticity in the volume, and $d\tau(\boldsymbol{r}_s)$ is the volume element at $\boldsymbol{r}_s$. When the vorticity is concentrated in a straight line, Eq. (3) reduces to the Biot-Savart law.

Equation (3) is a purely kinematical relationship; thus, it is valid for viscous as well as inviscid flowfields. The flowfield given by Eq. (3) is incompressible everywhere, and in the regions where $\boldsymbol{\Omega} = \boldsymbol{0}$, it is irrotational. Moreover, it follows from Eq. (3) that vorticity anywhere in the flowfield generates velocity everywhere in the flowfield; the familiar induced drag is a consequence. The goal is to find the function $\boldsymbol{\Omega}(\boldsymbol{r}_s, t)$ such that the vorticity in the boundary layers and wakes generates a velocity field that disturbs the freestream to the extent that the no-penetration condition is satisfied on the surface of the configuration.

In the present model of the flowfield, all the vorticity is assumed to be concentrated in the boundary layers adjoining

Received June 7, 1993; revision received Oct. 29, 1993; accepted for publication Oct. 30, 1993.

*Department of Engineering Science and Mechanics; currently at the Mathematics and Computer Department, United Arab Emirates University, Al-Ain, United Arab Emirates.

†Department of Engineering Science and Mechanics. Associate Fellow AIAA.

‡Department of Engineering Science and Mechanics. Fellow AIAA.

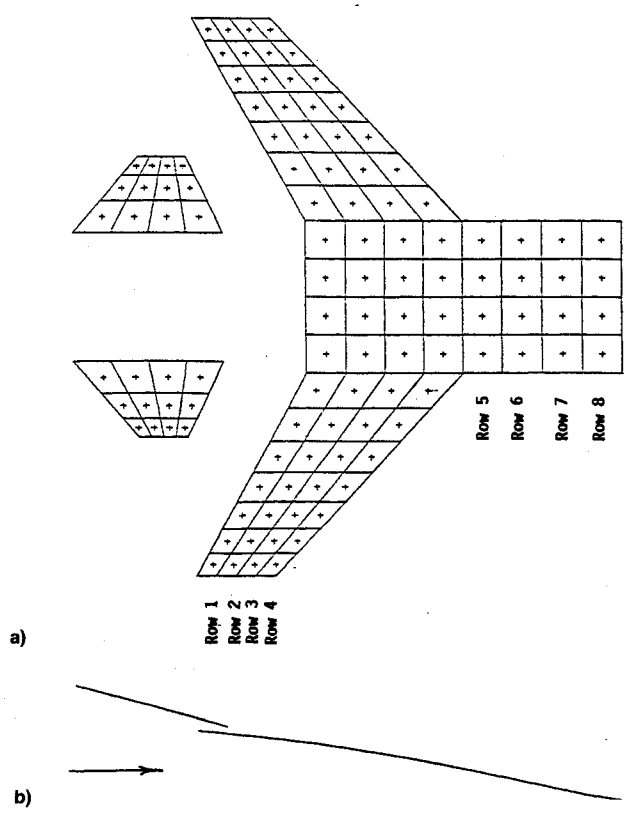

Fig. 1 Canard is at 15 deg and the main wing is at 9 deg with the freestream. The eight rows are identified here for the spanwise pressure distributions given in Fig. 4: a) is the lattice used to obtain all of the results presented in this article and b) is the side view showing the planar canards and cambered main wing.

the surfaces and in the wakes. Moreover, the wings are taken to be very thin so that the boundary layers on the upper and lower surfaces are merged to form a single vortex sheet, the lifting surface. The wake is also represented by a vortex sheet. No effects of thickness are included in the present model of the flowfield.

The vorticity distributions in the simulations of both the boundary layers and the wakes are further approximated by lattices consisting of short straight vortex segments. The segments are always grouped in such a way that they form closed four-sided elements, and to satisfy the requirement of spatial conservation of vorticity, the circulations around the four vortex segments of any given element are equal. Typically, each one of the vortex segments of a given element is coincident with one of the vortex segments of a neighboring element; the exceptions are the elements along the leading edges. At the centroid of the corners of a given element is a so-called control point, and associated with each element is an approximate normal vector obtained from the cross product of the two diagonals.

The lattice used to obtain the present results is shown in Fig. 1. The canards move together and are regarded as a single element. The canards have symmetric profiles, and the lattices representing them are planar. The main wing has cambered profiles, and the lattice representing it lies on the camber surface. We use three coordinate systems to keep track of the configuration: 1) one fixed to the ground, 2) one fixed to the canards, and 3) one fixed to the main wing. Communication among the three is by means of two sets of Euler angles.

The circulations for each element are obtained by simultaneously satisfying the no-penetration condition at all of the control points

$$\sum_{j=1}^{N} A_{ij}G_j = (\boldsymbol{V}_{ls_i} - \boldsymbol{V}_{w_i})\cdot \boldsymbol{n}_i \tag{4}$$

for $i = 1, 2, \ldots, N$, where N is the number of elements, A_{ij} is the normal component of the velocity at the control point of element i generated by the unit-circulation vortex segments of element j, G_j is the actual circulation around the four vortex segments that enclose element j, $\boldsymbol{V}_{ls_i}$ is the velocity of the control point (the aircraft is viewed as moving through still air), $\boldsymbol{V}_{w_i}$ is the velocity induced by the wake at the control point, and $\boldsymbol{n}_i$ is the unit normal vector.

The influence matrix A_{ij} is partitioned

$$\sum_{j=1}^{N} A_{ij}G_j \quad \text{for } i = 1, 2, \ldots, N \quad \text{is replaced with}$$

$$\begin{bmatrix} B_{11} & B_{12} \\ B_{21} & B_{22} \end{bmatrix} \begin{Bmatrix} F_1 \\ F_2 \end{Bmatrix} \tag{5}$$

where $[B_{11}]$ is the influence of the canards on themselves, $[B_{12}]$ is the influence of the main wing on the canards, $[B_{21}]$ is the influence of the canards on the main wing, and $[B_{22}]$ is the influence of the main wing on itself. When the canards and wing are considered rigid, as they are here, $[B_{11}]$ and $[B_{22}]$ do not change. When the canards are deflecting, $[B_{12}]$ and $[B_{21}]$ change and, hence, must be computed at each time step. $\{F_1\}$ and $\{F_2\}$ are the components of the G_j for the canards and the main wing, respectively.

At each time step, a so-called Kutta condition is imposed along the trailing edges and tips. Specifically, we render the pressure difference across the lattice zero along these edges. Although Eq. (3) is valid for viscous as well as inviscid flows, the present method is an "inviscid" one. What makes the present method inviscid is that we convect the vorticity in the wake at the velocity of the fluid particles and keep the circulation around a given vortex segment in the wake constant. For an inviscid flow, this procedure eliminates discontinuities in the pressure and, hence, renders the wake force-free.

To impose the Kutta condition, we convect the vortex segments along the trailing edges and tips away from the wings at the local particle velocity; the process is often called vorticity shedding and the vorticity released in this way is often called shed vorticity. As one vortex segment is shed, another forms, and those already in the wake are convected at the local particle velocity a little farther downstream. At the beginning of each time step the velocities at all the nodes in the wake are computed. The velocities include contributions from the vorticity in the lattices representing the canards and the main wing as well as vorticity in the wakes of these components. There could also be a contribution from the wind, although the aircraft is viewed as moving through the air rather than being in a freestream. Then, each node is moved according to the following explicit algorithm:

$$\boldsymbol{r}(t + \Delta t) = \boldsymbol{r}(t) + \boldsymbol{v}[\boldsymbol{r}(t)]\Delta t \tag{6}$$

where $\boldsymbol{r}$ is the position of a given node and $\boldsymbol{v}$ is the velocity. Numerical experiments with more accurate, more time-consuming algorithms have shown this to be sufficiently accurate and stable. After a vortex segment is shed into the wake, the circulation around it does not change.

The vorticity presently in the wake was shed previously; thus, what is happening now depends to some extent on what happened earlier. The flowfields are history-dependent and the "historian" of the flow is the wake. Indeed, this property of general unsteady vortex-lattice methods was the key to the accurate numerical and analytical simulations of the subsonic wing-rock phenomenon for slender delta wings achieved earlier.[2-6]

In the present simulations of the flowfield we assume that wakes are attached to both ends (or tips) and to the trailing edge of each canard (the canards sit out a short distance from the fuselage in the actual aircraft), and along all but the leading edges of the main wing. The wakes are generated as part

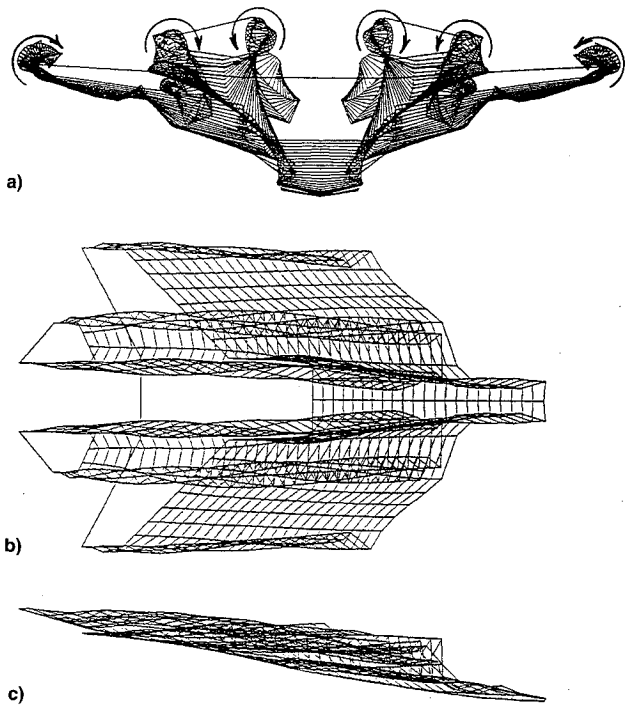

Fig. 2 Computed wakes for the configuration shown in Fig. 1: a) rear view, b) top view, and c) side view. The configuration is at 9-deg angle of attack, and the canards are deflected 6 deg (their angle of attack is 15 deg). The heavy curved arrows in part a) indicate the direction of the flow induced by the various tip vortex systems.

of the solution. An example of the computed wakes for the configuration in Fig. 1 is given in Fig. 2.

Because the elements of the lattices representing the wing and canards (the lifting surfaces) have specified positions, there is a discontinuity or jump in the value of the pressure across these portions of the lattices. After the G_j are found, these pressure differences are computed from the unsteady Bernoulli equation, then the pressure differences are multiplied by the areas and unit normals to produce the forces on the elements, and finally the elemental forces and their moments are summed vectorially. No leading-edge suction effects are included in any of the force calculations. For more details on the basic approach, see Konstadinopoulos et al.[7]

Constant-circulation vortex segments along the edges of a planar element generate the same velocity field as a constant-strength distribution of doublets over the surface of the element. Hence, any of the numerous popular doublet-panel methods, if they accurately and robustly account for the shedding and subsequent convection of vorticity in the wake, will produce results similar to those presented here. Our purpose here is to illustrate the capabilities of this class of methods; we do not imply a claim that our version of such a general approach is the only possibility. We do emphasize, however, that any attempt to model flowfields such as those considered here must include accurate, robust predictions of the wake.

III. Results

Some numerical results for both steady and unsteady flows are discussed in this section. All of the results were obtained with the same code, which models general unsteady flows. Steady flows may be regarded as a special case. To obtain a steady flow, we first give the configuration an impulsive start, and then have it translate at constant velocity until the steady state develops.

A. Steady Flows

In the first example, the canards are undeflected and the entire configuration is placed at various angles of attack. It is possible to select a single characteristic area and compute

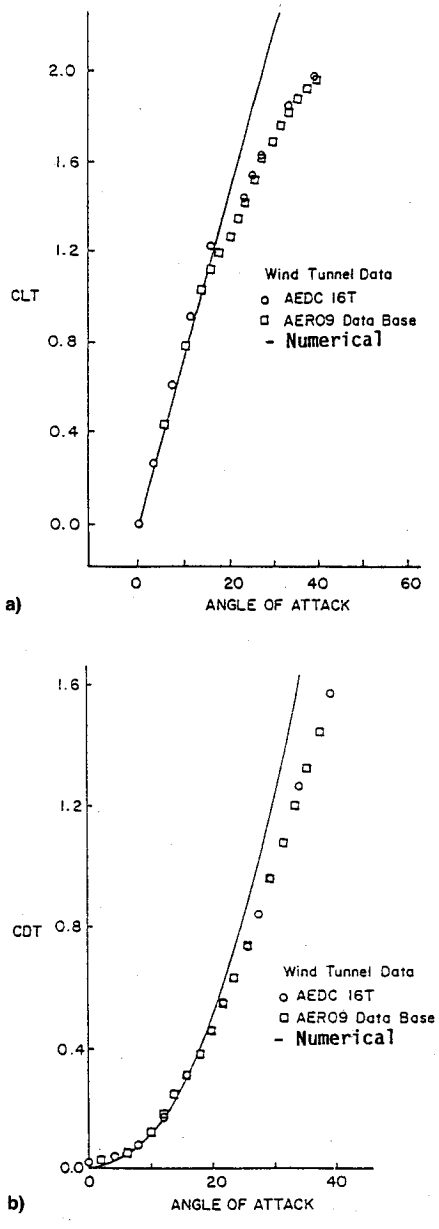

Fig. 3 Total load coefficients as functions of angle of attack of the main wing: a) lift and b) drag coefficients for the complete configuration. The canards are not deflected.

lift and drag coefficients. We selected the area that produced agreement between the calculated and wind-tunnel lift coefficients at 5-deg angle of attack, and then used the same area to compute the drag and lift coefficients at all angles of attack. (This area is nearly equal to the area of the lattices shown in Fig. 1.) The results are shown in Fig. 3; see Ref. 8. It appears that around 20-deg angle of attack some sort of partial stall occurs and the numerical results begin to overpredict the lift substantially. Only drag due to lift is calculated, which appears to be responsible for nearly all of the drag. It is surprising that the crude numerical model of the X-29 given in Fig. 1 can produce such a good imitation of an actual model of the X-29 in the wind tunnel.

To illustrate how significant the aerodynamic interference is, we plotted the distributions of pressure differences across the lifting surface approximating the main wing ΔC_p. The differences were found at each control point in the lattice shown in Fig. 1, and a spline was placed through the results along the eight spanwise rows of elements shown. The pressure differences are given in Fig. 4.

In Fig. 4a, the planforms of the canards and main wing and the wakes emanating from the canards are shown. The wake

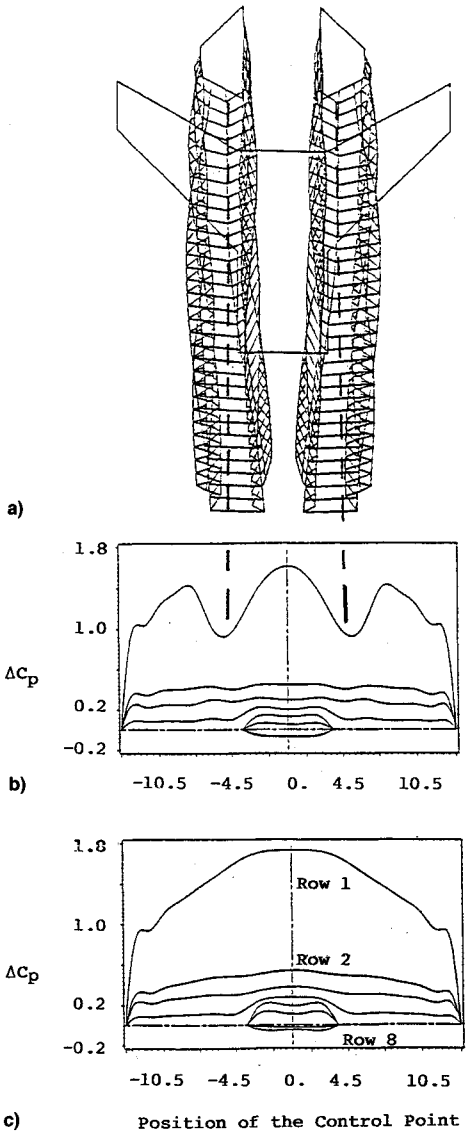

Fig. 4 Configuration is at 15-deg angle of attack, and the canards are not deflected. The heavy dashed lines are to aid in determining the location of the large pressure loss with respect to the wakes. The locations of the control points in each spanwise row of the main-wing lattice are given in Fig. 1: a) show the wakes of the canards, b) the pressure difference across the main wing when the canards are in place, and c) the pressure difference across the main wing when the canards are removed.

of the main wing has been removed in order to simplify the picture. In Fig. 4b the variations of the pressure differences along the various spanwise rows are shown when the canards are in place. The heavy dashed lines are to help position the large pressure loss with respect to the wakes.

In Fig. 2a, the flow around the tip vortices of the canards is indicated by the heavy curved arrows. There is a strong downwash induced on the main wing in the regions between the two tip vortices of a given canard, and a mild upwash induced everywhere else. The strong downwash is responsible for a large loss in sectional lift for the portion of the main wing between the two tip vortices. The mild upwash is responsible for a rise in lift for the outboard portion of the main wing. When the main wing is at a high angle of attack, the strong downwash induced by the canards could keep the boundary layers on a portion of the main wing attached while those on the rest of the main wing are separating. Because the canards have a small aspect ratio, their boundary layers most likely will not experience separation until the canards reach relatively high (20- to 25-deg) angles of attack. Determining accurate estimates of the strength, orientation, and location of the vorticity in the wakes of the canards is essential to determining accurate estimates of the lift and drag on the main wing.

In Fig. 4c, the pressure differences on the main wing are shown after the canards have been removed. Comparing the results in Figs. 4b and 4c, one can see the strong influence that the wakes of the canards have on the main wing. Evidence of the wingtip vortex systems of the main wing can also be seen in Figs. 4b and 4c. As expected, the biggest pressure difference occurs near the leading edge. One can see that the Kutta condition is satisfied and that very little load is carried by the last four rows of the center plate of the main wing.

As another example to illustrate the significance of the aerodynamic interference in this configuration, we consider the situation in which the main wing is held fixed at 9-deg angle of attack, while the canard is set at three deflections (δ_c = 1, 6, and 11 deg). The results are given in Table 1. As the deflection of the canards increases and their tip vortex systems grow stronger, the lift and drag on the main wing decrease. The canards qualitatively exhibit expected behavior—lift and drag increase. The complete configuration experiences almost no change in lift, a modest increase in drag, and a marked increase in the pitch moment.

When the canards and main wing operate alone, the lift and drag coefficients are given in Table 2. Comparing these results with the middle line of Table 1, we see that one has considerable influence on the other. Moving the canards close to the main wing causes the lift on them to rise substantially, from a C_L of 0.56 to a C_L of 0.65, with an expected increase in drag. This can be explained by the fact that the strong spanwise vorticity of the main wing creates an upwash on the canards and, hence, increases the apparent angle of attack. Moreover, the forward sweep of the main wing tends to focus the induced upwash on the canards; a rearward sweep would tend to weaken, or diffuse, the induced upwash. The spanwise vorticity of the canards has the opposite effect on the main wing, and the wakes of the canards produce an additional downwash, as discussed above.

We emphasize that the numerical simulation of the flowfield presented here does not model stall and, consequently, is valid only at angles of attack below 20 deg approximately. Ericsson[9] included the X-29 in his recent discussion of the wing-rock phenomenon, and attributed the loss in roll damping to the "moving-wall effect." Briefly, the moving-wall effect enhances the separation (stall) on the wing during the downward motion and retards it during the upward motion; thus, in the incipient-stall regions of the flight envelope, a perturbation in roll will be unstable and lead to a rolling motion. The rolling motion is arrested when the effective angle of attack of the downward-rolling wing is reduced to the point where the flow reattaches and high lift is restored. The reader is referred to

Table 1 Force coefficients for the canards, main wing, and complete configuration

	Canard		Main wing, α = 9 deg		Complete configuration		
δ_c	C_L	C_D	C_L	C_D	C_L	C_D	C_P
1	0.401	0.071	0.401	0.053	0.401	0.055	0.0079
6	0.651	0.174	0.385	0.050	0.420	0.067	0.0187
11	0.981	0.334	0.355	0.046	0.430	0.085	0.0318

Table 2 Force coefficients for the main wing and canards when they are separated

Canard, δ_c = 6 deg, α = 15 deg		Main wing, α = 9 deg	
C_L	C_D	C_L	C_D
0.559	0.150	0.450	0.060

Ericsson's paper for a more thorough discussion. Fratello et al.[10] observed negative roll damping and wing rock in both wind-tunnel and drop tests. In other wind-tunnel tests, Brandon and Nguyen[11] observed that a more violent wing-rock can be the result of asymmetric vortices shedding from the forebody.

An interesting consequence of the downwash generated by the canards on the main wing is that separation occurs on the outboard sections of the wing before it occurs on the inboard sections. Hence, the canards, which degrade the lift when there is no separation, enhance the lift after separation begins.

B. Unsteady Flows

In the first example, the angle of attack of the canard is smoothly ramped up from 15 to 18 deg, as shown in Fig. 5a. (The actual function is one-quarter of a sine wave.) The angular velocity of the canards is shown in Fig. 5b. The angle of attack of the main wing remains fixed at 9 deg. The normal-force coefficient for a canard and the lift coefficient for the main wing are shown in Fig. 5c. After the motion stops, the C_N quickly converges to the correct steady-state value. The

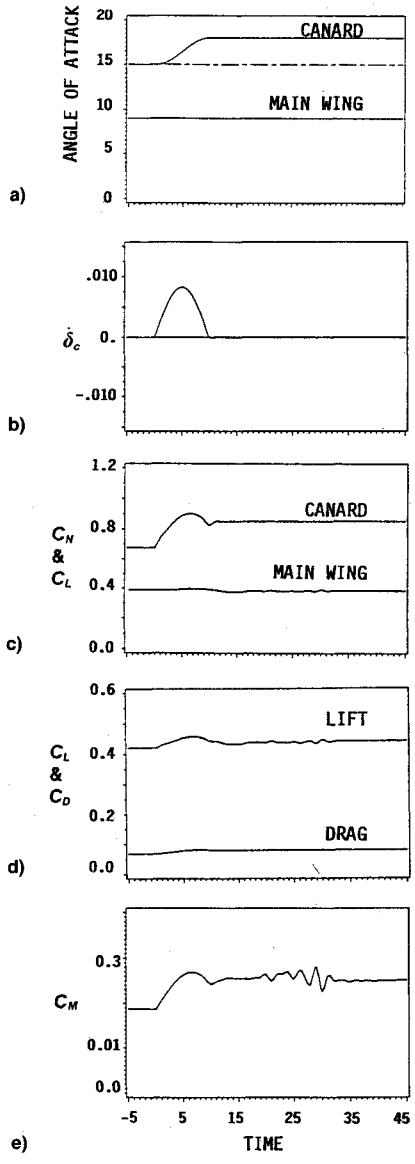

Fig. 5 Results for a smooth ramp from 15- to 18-deg angle of attack of the canards: a) angles of attack; b) angular velocity; c) normal-force coefficient for the canard and lift coefficient for the main wing; d) lift and drag coefficients for the complete configuration; and e) pitch-moment coefficient, all as functions of dimensionless time.

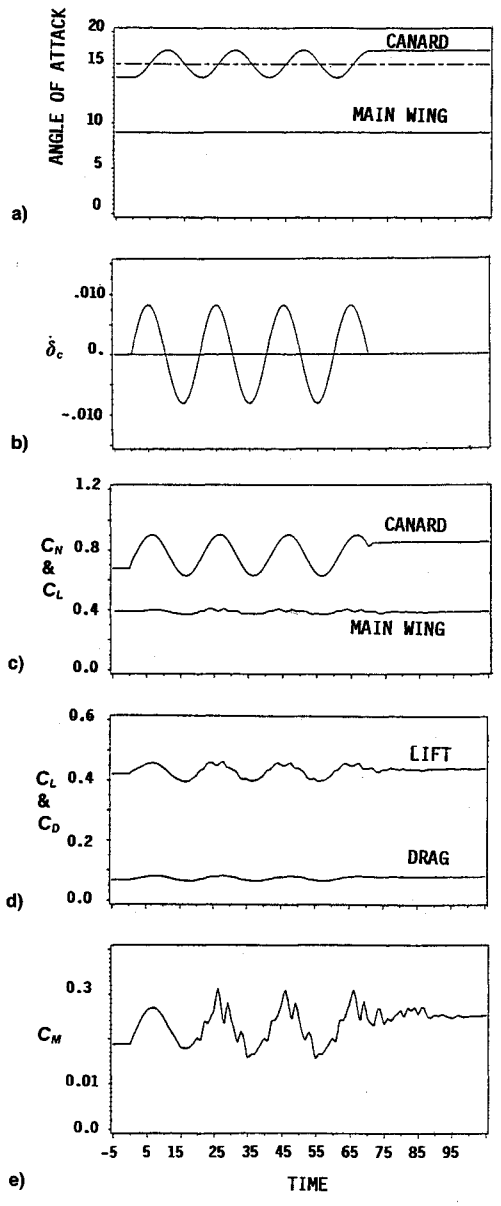

Fig. 6 Results for three and one half cycles of simple-harmonic motion of the canards: a) angles of attack; b) angular velocity; c) normal-force coefficient for the canard and lift coefficient for the main wing; d) lift and drag coefficients for the complete configuration; and e) pitch-moment coefficient, all as functions of dimensionless time.

maximum of the C_N occurs slightly after the maximum of the velocity occurs. The force on the main wing changes slightly, first rising a little and then decreasing. The lift and drag on the complete configuration are given as functions of dimensionless time in Fig. 5d. The maxima of the lift and drag occur simultaneously, approximately when the angular velocity of the canards reaches its maximum. The small fluctuations visible in the lift between the dimensionless times of 20–30 occur when the strong vorticity released from the canard passes directly over the main wing. Because of the discretization, the modeling of this passage of vorticity appears a little erratic. In reality, some very small and very brief buffeting should be expected because of the turbulence in the wake. However, we emphasize that the present approach does not simulate buffeting, but only indicates when and where buffeting is likely to occur. The erratic behavior is more visible in the plot of the pitch-moment coefficient as a function of time in Fig. 5e because of the scale. The maximum of the pitch moment occurs approximately when the maximum of the velocity occurs. The time between when the large change in pitch occurs and when the erratic behavior is visible is the time required

for the strong vorticity shed from the canard to convect downstream to the main wing. This strong shed vorticity does not clear the main wing until the dimensionless time = 35 approximately. The moment at time = 15 is not quite the same as the moment at time = 35.

In the second example, the canards execute three and one-half cycles of a simple harmonic motion around 16.5-deg angle of attack, and then freeze at 18-deg angle of attack. As before, the main wing remains fixed at 9-deg angle of attack. The angle of attack is plotted as a function of time in Fig. 6a; the angular velocity is plotted in Fig. 6b. In Fig. 6c, the normal force on the canard and the lift on the main wing are given as functions of time. Small erratic fluctuations, similar to those seen above, appear in the load on the main wing. As mentioned above, these fluctuations occur when the wakes of the canards pass closely by the main wing. No wakes pass directly over the canards, which do not experience any noticeable fluctuations. The lift and drag on the complete configuration are given in Fig. 6d, and the pitch moment is plotted in Fig. 6e. For the first cycle, the lift and pitch moment are free of fluctuations because the wakes from the canards have not yet reached the main wing. The maxima of the normal force on the canard, lift, drag, and pitch moment all occur about the same time in the cycle, which is a little after the maximum of the angular velocity and somewhat before the maximum of the angle of attack of the canards. Although the motion of the canards stops around dimensionless time = 70, the steady state does not arrive until time = 100 approximately. Finally, it appears that a steady-state, oscillatory response to the motion of the canards has developed by the end of the first cycle.

IV. Concluding Remarks

The present results illustrate the need to model the wakes accurately in simulations of both steady and unsteady aerodynamic interference. Thus, for any model of the flow to be successful, it must accurately predict both the rate at which vorticity is being shed from the lifting surfaces into the wakes, and the way in which the shed vorticity is being transported after it enters the wake. The general unsteady vortex-lattice model of the flowfields treats the wake as an inviscid, rotational flow, and vorticity is transported at the local fluid-particle velocity. The rate at which vorticity is shed into the wake is determined by requiring the difference in the pressures on the upper and lower sides of a lifting surface to vanish along the edges that are joined to the wakes. In general, the time-dependent strength, orientation, and location of the vorticity in the wake are part of the solution. All of the solutions are obtained from the same code; steady states are simply special cases and obtained by giving the configuration an impulsive start and then having it translate at constant velocity until the steady state emerges.

The present results show that the wakes of the canards as well as the canards themselves have a very strong negative influence on the lift generated by the main wing. In contrast, the main wing has a positive influence on the lift generated by the canards; moreover, the forward sweep of the main wing tends to focus the upwash it generates on the canards and, consequently, enhances its influence. As a result of this interaction, changing the incidence of the canards has almost no effect on the lift generated by the complete configuration: the positive (negative) change in the lift on the canards is nearly balanced by the negative (positive) change in the lift on the main wing when the incidence of the canards is changed. In the examples of unsteady flow, the present results show that the vorticity shed from the canards exerts a changing influence on the main wing as it convects downstream. The importance of simulating the wakes accurately in any model of vorticity-dominated, strongly interfering flowfields is demonstrated, and the general unsteady vortex-lattice method is shown to be a good candidate for, at the least, preliminary studies of such flows and subsequent simulations of the flying qualities of configurations featuring such unsteady interference.

Acknowledgments

This work was supported by the Air Force Office of Scientific Research under Grant AFOSR-90-0032. We are indebted to Lars Ericsson for several comments that were incorporated into the present manuscript.

References

[1]Elzebda, J., Mook, D. T., and Nayfeh, A. H., "Unsteady Aerodynamic Interference for Lifting Surfaces," AIAA Paper 85-1801, Aug. 1985.

[2]Konstadinopoulos, K., Mook, D. T., and Nayfeh, A. H., "Subsonic Wing Rock of Slender Delta Wings," *Journal of Aircraft*, Vol. 22, No. 3, 1985, pp. 223–228.

[3]Elzebda, J. M., Nayfeh, A. H., and Mook, D. T., "Development of an Analytical Model of Wing Rock for Slender Delta Wings," *Journal of Aircraft*, Vol. 26, No. 8, 1989, pp. 737–743.

[4]Nayfeh, A. H., Elzebda, J. M., and Mook. D. T., "Analytical Study of the Subsonic Wing-Rock Phenomenon for Slender Delta Wings," *Journal of Aircraft*, Vol. 26, No. 9, 1989, pp. 805–809.

[5]Elzebda, J. M., Mook, D. T., and Nayfeh, A. H., "Influence of Pitching Motion on Subsonic Wing Rock of Slender Delta Wings," *Journal of Aircraft*, Vol. 26, No. 6, 1989, pp. 503–508.

[6]Mracek, D. T., and Mook, D. T., "Aerodynamic Potential Flow Panel Method Coupled with Dynamics and Controls," AIAA Paper 91-2846, Aug. 1991.

[7]Konstadinopoulos, K., Thrasher, D. F., Mook, D. T., Nayfeh, A. H., and Watson, L., "A Vortex-Lattice Method for General, Unsteady Aerodynamics," *Journal of Aircraft*, Vol. 22, No. 1, 1985, pp. 43–49.

[8]Mook, D. T., and Nayfeh, A. H., "Numerical Simulations of Dynamic/Aerodynamic Interactions," *Symposium on Computational Technology on Flight Vehicles*, in *Computing Systems in Engineering*, Vol. 1, Nos. 2–4, 1990, pp. 461–482.

[9]Ericsson, L. E., "Various Sources of Wing Rock," *Journal of Aircraft*, Vol. 27, No. 6, 1990, pp. 488–494.

[10]Fratello, D. J., Croom, M. A., Nguyen, L. T., and Domack, C. S., "Use of the Updated NASA Langley Radio-Controlled Drop-Model Technique for High-Alpha Studies of the X-29A Configuration," AIAA Paper 87-2559, 1987.

[11]Brandon, J. M., and Nguyen, L. T., "Experimental Study of Effects of Forebody Geometry on High Angle-of-Attack Stability," *Journal of Aircraft*, Vol. 25, No. 7, 1988, pp. 591–597.